Heliyon 9 (2023) e18638

Contents lists available at ScienceDirect

Heliyon

journal homepage: www.cell.com/heliyon

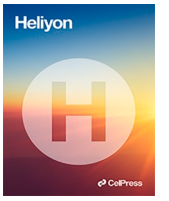

Combined operando and ex-situ monitoring of the Zn/electrolyte interface in Zn-ion battery systems

Pornnapa Phummaree [a,1], Manaswee Suttipong [a,b,1], Theeraboon Jaroonsteanpong [a], Catleya Rojviriya [c], Rojana Pornprasertsuk [b,d,e], Soorathep Kheawhom [e,f], Jitti Kasemchainan [a,b,e,*]

[a] Department of Chemical Technology, Faculty of Science, Chulalongkorn University, Bangkok, 10330, Thailand
[b] Center of Excellence on Petrochemical and Materials Technology, 7th floor, Chulalongkorn University Research Building, Soi Chula, 12, Phayathai Rd, Bangkok, 10330, Thailand
[c] Synchrotron Light Research Institute (Public Organization), Nakhon Ratchasima, 30000, Thailand
[d] Department of Material Science, Faculty of Science, Chulalongkorn University, Bangkok, 10330, Thailand
[e] Center of Excellence on Advanced Materials for Energy Storage, Faculty of Science, Chulalongkorn University, Bangkok, 10330, Thailand
[f] Department of Chemical Engineering, Faculty of Engineering, Chulalongkorn University, Bangkok, 10330, Thailand

ARTICLE INFO

Keywords:
Operando optical microscopy
Synchrotron X-ray imaging
Surface characterization
Zn-ion batteries
SiO_2 additive
Zn/electrolyte interface

ABSTRACT

Operando optical microscopy enables imaging at the interface between the Zn electrode and the electrolyte of 1 M $ZnSO_4$(aq) in the symmetrical Zn/Zn cells assembled as the pouch cells with the mechanical load of 0.8 MPa. The imaging was executed during cycling of Zn plating and stripping at the different current densities of 0.5, 1.0, 2.0, and 4.0 mA cm^{-2}, and the areal capacity of 2 mAh·cm^{-2}. When the current densities are below 4.0 mA cm^{-2}, no intense Zn dendrites are observed. However, at 4.0 mA cm^{-2}, the severe Zn dendrites can penetrate through the separator and cause short-circuiting. From the electrochemical perspective, the voltage profile of such system drops to almost zero volt. Both operando optical and ex-situ synchrotron X-ray imaging further prove the appearance of the Zn dendrites. By Raman spectroscopy and X-ray diffraction, the cycled Zn electrode surface contains passivation species of $Zn_4(OH)_6SO_4$, ZnO, and $Zn(OH)_2$ that could limit the active surface area for the Zn plating/stripping, accelerating the localized current density and favoring the growth of Zn dendrites. With the SiO_2 additive of 0.5% w/v in 1 M $ZnSO_4$(aq), the severe Zn dendrites disappear, as well as the cycled Zn/electrolyte interface becomes close to the pristine state; low degree of the Zn electrode roughness and the Zn surface passivation is noticed. The appearance of the claimed Zn surface morphology was also confirmed by Scanning Electron Microscopy (SEM). In turn, too low or too high SiO_2 content in the electrolyte does not generate desirable effects. A high level of Zn dendrites and short circuiting are still recognized. Hence, both the operando and ex-situ characterizations can mutually validate the phenomena at the Zn/electrolyte interface.

* Corresponding author. Department of Chemical Technology, Faculty of Science, Chulalongkorn University, Bangkok, 10330, Thailand.
E-mail address: jitti.k@chula.ac.th (J. Kasemchainan).
[1] These authors contribute equally.

https://doi.org/10.1016/j.heliyon.2023.e18638
Received 20 June 2023; Received in revised form 19 July 2023; Accepted 24 July 2023
Available online 27 July 2023

1. Introduction

Zn-ion batteries (ZIBs) are among promising rechargeable batteries that use zinc as the anode material instead of lithium metal or lithium compounds in the more common and developed Lithium-ion batteries (LIBs). Zinc is a much more abundant and less expensive material than lithium, which makes ZIBs potentially more cost-effective and environmentally friendly. Additionally, ZIBs have a higher energy density to become a viable alternative to LIBs in some applications, including portable electronics and grid storage. However, several challenges still need to be improved in the efficiency and stability of ZIBs, particularly related to zinc dendrite formation, corrosion, and irreversible side reactions [1–3]. In subsequent stripping processes, Zn dendrites may break from the roots forming the so-called "dead Zn". Moreover, due to the intrinsic inhomogeneous nature of Zn metal and its uncontrolled deposition behaviour, Zn ions prefer to deposit on the tip spots because of fast reaction kinetics and shorter diffusion length [4]. Since the emergence of ZIBs, research on the interfacial phenomena between Zn electrode and electrolyte such as Zn-dendritic formation/growth, Zn-corrosion, as well as Zn-passivation have been mainly in focus in order that what cause(s) the phenomena and how to prevent them can be well-defined. Operando and/or In-situ characterizations have been deemed a powerful technique that is capable of unravelling those phenomena. They can detect the "real-time" alteration of the Zn/electrolyte interfacial morphology [5–9]. For example, Banik et al. studied the zinc electrodeposition in KOH electrolyte containing polyethyleneimine (PEI) additive [10], and Vladimir et al. utilized the in-situ observation technique to provide insights into zinc dendrites formation and dissolution mechanism in alkaline solutions by synchrotron X-ray computed tomography (SXCT) [11]. Recently, Cai et al. investigated morphologies during zinc electrodeposition from $ZnSO_4$ electrolytes at high current densities [12]. However, these prior studies of the zinc dendrite formation were with neither the presence of the separator nor the applied external mechanical load, which were in fact not real operation appearing in any batteries. Furthermore, the chemical composition and structure of the surface electrode using Fourier transform infrared (FTIR), Raman spectroscopy, and X-ray diffraction (XRD) indicates byproducts (e.g., ZnO, $Zn(OH)_2$, $Zn_4(OH)_6SO_4$ and alkaline Zn salt) [13–18].

Regarding additives in the Zn-ion batteries, polymer-based compounds have been widely studied and developed for ZIBs. Composites polymer electrolytes comprise a polymer host, doping inorganic salt and ceramic filler. The polyethylene oxide (PEO) with $ZnSO_4$ was found to have an excellent coulombic efficiency (CE) of 99.5% over 3000 h Zn plating/stripping cycles [19] due to high molecular weight PEO. Benefitting from these low molecular weight PEG, the Zn anode in electrolyte with PEG additive achieved high cyclic performance for 9000 or 8000 h at 1 or 2 mA cm^{-2} [20]. Nevertheless, the use of composite electrolytes can still be a challenge. Additionally, the use of inorganic fillers into the separator and/or the polymer electrolytes (such as TiO_2 [21], ZrO_2 [22], Al_2O_3 [23, 24], SiO_2 [25,26] can effectively reduce the crystallinity of the polymer to improve the ionic conductivity and the mechanical properties, and to suppress the dendrites; however, their influence on the Zn electrode surface phenomena is rarely researched, especially in case of adding SiO_2 directly into the liquid electrolyte.

Moreover, it was reported that adding some liquid and solid additives into aqueous electrolytes in Zn-ion batteries such as ethylene glycol, dimethyl sulfoxide, ammonium chloride, and ethylamine hydrochloride, was able to manipulate the electrolyte solvation structure, so that the parasitic reactions, e.g. hydrogen evolution, surface passivation, and dendrite formation, were suppressed [27–35]. In general, the additive molecules should contain strong polar electron-donors like oxygen and nitrogen to coordinate with Zn^{2+}; at the same time, they can replace the water molecules solvating Zn^{2+}. These solvating water molecules were believed to be chemically active and responsible for any undesirable reactions with the metallic Zn electrodes. Provided that the number of the solvating water molecules is decreased, the reactions will be automatically deactivated. The Zn electrodes will be thus more stable and subsequently the Zn plating and stripping processes will happen smoothly and continually.

This research will focus on addressing the issues at the interface of the Zn electrode associated with the aqueous electrolytes by "operando" optical monitoring. As not in the previous works, it will enable insight investigation during the Zn plating and stripping processes that occur in the real time of the Zn/Zn cell operation, where the pouch cells with an external mechanical load was applied. We will also provide systematic investigation on the variation of the current densities and the SiO_2 additive quantities: 1 M $ZnSO_4$ + x % w/v – x = 0.1, 0.5, 1, 5, or 10, in Zn/Zn symmetrical cells on how they can influence and suppress the Zn dendritic formation and growth. Other "ex-situ" techniques such as synchrotron X-ray imaging, Raman spectroscopy, X-ray diffraction, and Scanning electron microscopy, will be further exploited to reveal the Zn dendritic growth, and the Zn electrode surface corrosion and passivation species.

2. Materials and methods

2.1. Preparation of Zn electrodes and electrolytes

The 100-μm thick Zn foils (China Stainless steel, 99%) were cut into circular electrodes having a diameter of 4.0 mm. The Zn electrodes were immersed in 0.5 M CH_3COOH(aq) (Qrec, 98%) for 30 min, followed by washing with deionized water and quick drying with a hot-air blower. The base aqueous electrolytes were prepared by homogeneously mixing $ZnSO_4{\cdot}7H_2O$ (Kemaus, >99%) and deionized water to reach the concentration of 1 M $ZnSO_4$(aq). In addition, different amount of fumed SiO_2 (Sigma-Aldrich, Analytical Grade), i.e. 0.1, 0.5, 1, and 10% w/v was added to obtain another system of the liquid electrolyte so as to study the effects of this additive.

2.2. Assembly of symmetrical Zn/Zn battery cells

A piece of Polypropylene (PP) with the thickness of 2 mm was used as the separator. The aqueous electrolytes with or without the SiO_2 additive were added to soak up the separator. After stacking two zinc electrodes with the electrolyte-soaked separator in the

middle, each stripe of stainless steel, serving as an electrical conductor, was attached to each zinc electrode. All the components were inserted in a (vacuum-sealer) transparent bag before being vacuum-sealed, giving an enclosed pouch cell of a symmetrical Zn/Zn battery cell. A mechanical load of *ca.* 0.8 MPa was applied on the cell. A schematic of the cell is represented in Fig. 1.

2.3. Electrochemical tests

Zn plating or stripping processes at the interface between the Zn electrode and the electrolyte (separator) in the Zn/Zn symmetrical cells were activated according to the imposition of a constant current. Both plating and stripping happened simultaneously; when stripping took place at a Zn electrode, plating occurred at the other one. The current imposition was performed forward and backward iteratively with the number of cycles or so-called as Galvanostatic cycling. The current densities per the planar area of the Zn electrode were applied at 0.5, 1.0, 2.0, and 4.0 mA cm^{-2} for the cells with the 1 M $ZnSO_4$(aq) electrolyte and 4.0 mA cm^2 for the cells with the 1 M $ZnSO_4$(aq) + x % w/v SiO_2 electrolyte. The areal capacity was always fixed at 2.0 mAh·cm^{-2} for each direction of the current applied, or 4.0 mAh·cm^{-2} per cycle. These electrochemical measurements were carried using a Neware battery tester (CT-4008T-5V, 20 mA). The cell voltage profile was plotted versus time to depict the plating and stripping behavior from the cycling data.

2.4. Operando and ex-situ characterizations

To operando-wise inspect the morphological change at the interface between the Zn electrode and the electrolyte in the Zn/Zn cells at the time of the galvanostatic cycling with 0.5, 1.0, 2.0, and 4.0 mA cm^{-2}, an optical microscope with 5-times magnification of the objective lens (Nuvotech, Model TR3-1) was operated. The characterized Zn/Zn cells were of either 1 M $ZnSO_4$(aq) or 1 M $ZnSO_4$(aq) + x % w/v SiO_2. The optical images at the interface were captured during the 1st, 10th, 25th, 50th, and 100th cycle of plating and stripping.

As for the ex-situ characterizations, four techniques were employed: i) synchrotron X-ray imaging (Multipole wiggler 2.4 T) to visualize the Zn dendritic growth through the separator, ii) Raman spectroscopy (PerkinElmer, Spectrum GX, 532 nm laser) to examine the chemical functional groups on the Zn electrode surface, iii) X-ray diffraction (XRD – Bruker D8 Advance) to verify the crystalline compounds formed at the Zn electrode surface, and iv) Scanning electron microscopy (SEM – JEOL, JSM-6610LV – 15 kV) to view the surface morphology of the Zn electrode. After 10, 50, and 100 cycles of the galvanostatic cycling at all the current densities mentioned, the Zn/Zn cells with the electrolyte of 1 M $ZnSO_4$(aq) were dismantled, and the stack of Zn/separator/Zn was carefully taken for analysis by synchrotron X-ray imaging. Note that the cells with the electrolyte containing SiO_2 were not analyzed by the absorption-contrast X-ray imaging as the electron density and atomic structure of Si and Zn are very close; thus, both elements have similar absorption energies [36]. Accordingly, it was not possible to visualize the X-ray absorption contrast between Zn dendrites and SiO_2 particles. Further, the Zn/Zn cells with or without 1 M $ZnSO_4$(aq) + 0.5% w/v SiO_2 that were cycled at 4.0 mA cm^{-2} were disassembled and the Zn electrode was brought for surface analysis at the side that was in contact with the electrolyte-soaked separator by Raman spectroscopy and XRD. Further, SEM was employed to have images of the Zn electrode surface taken from the Zn/Zn cells with either 1 M $ZnSO_4$(aq) or 1 M $ZnSO_4$(aq) + 0.5% w/v SiO_2 after being cycled at 4.0 mA cm^{-2} for 50 cycles.

3. Results and discussion

Plating/stripping processes of Zn at the interface between the Zn electrode and the electrolyte can be related to the voltage polarization plotted against the cycling time when imposing a constant current onto the Zn/Zn symmetrical cells. Thanks to the fixed areal capacity of 2.0 mAh·cm^{-2}, different current densities of 0.5, 1.0, 2.0, and 4.0 mA cm^{-2} link to different times of 4, 2, 1, and 0.5 h,

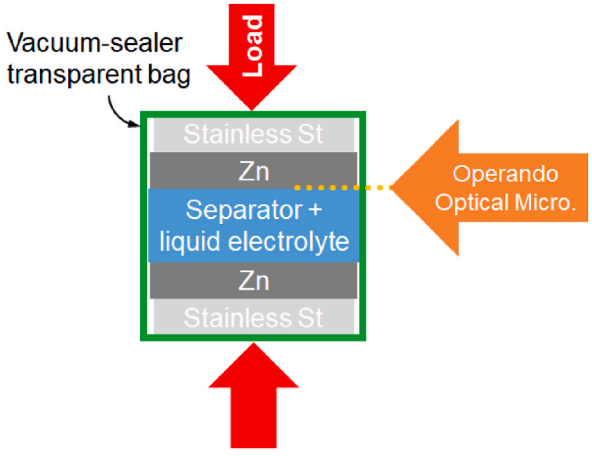

Fig. 1. Schematic representation of Zn/Zn symmetrical cells for electrochemical tests and characterization by operando optical microscopy.

respectively for each direction. From Fig. 2 (a) to (c) where the applied current densities were 0.5, 1.0, and 2.0 mA cm^{-2}, together with the electrolyte used was 1 M $ZnSO_4$(aq), the measured voltage is relatively stable versus the time. Aside from this, the positive and negative voltage magnitudes are almost identical. Note that the respective total cycling time for each current density of 0.5, 1.0, or 2.0 mA cm^{-2} is 1600, 800, or 400 h, which is equivalent to 200 cycles. These imply that the Zn plating and stripping processes reversibly occurred when the current densities range from 0.5 to 2 mA cm^{-2} throughout 100 cycles. In case of the highest current density of 4.0 mA cm^{-2}, the voltage profile in Fig. 2 (d) does illustrate otherwise (the electrolyte remained 1 M $ZnSO_4$(aq)). In the beginning of the cycling test or before 30 h or 30 cycles, the voltage polarization follows a slightly downward trend, meaning that the cell resistance is decreasing very likely caused by the formation and the growth of Zn dendrites.

When the test is about to accomplish 30 cycles, the voltage drops closely to 0 V (vs. Zn/Zn^{2+}), which refers to the fact that the cell has around zero-resistance. Generally accepted, this circumstance corresponds to direct contact between the two Zn electrodes via Zn dendrites acting as metallic wires for electron conductive pathways, also known as electrical short-circuiting. These results are in accordance with several works [4,10,11,19] that the higher current density is applied, the less uniform Zn deposition at the interface between the Zn electrode and electrolyte takes place, accelerating the formation and growth of Zn dendritic structure. How microstructure of the Zn/electrolyte interface alters when testing the Zn/Zn cells with different current densities will be discussed later.

Since high current densities are preferred in battery applications, x % w/v SiO_2 was added into the 1 M $ZnSO_4$(aq) electrolyte in an attempt to mitigate the issue of Zn dendrites as well as to study how this additive influences the phenomena at the Zn/electrolyte interface when the Zn/Zn cells were cycled at 4.0 mA cm^{-2}. The time-dependence-voltage curves of all the cells with different quantities of SiO_2 – 0.1, 0.5, 1.0, 5.0, and 10.0% are shown in Fig. 3. The electrolyte systems using 0.1 and 10.0% w/v SiO_2 as in the respective Fig. 3 (a) and 3 (e) suggest that the amount of SiO_2 is either too low or too high to be effective in improving the cycleability of the Zn/Zn cells at such a high current density. The voltage polarization of both systems decreases to nearly zero at around the same time of 50 h or 50 cycles after being cycled. In other words, they have similar short-circuiting behavior to the system with the electrolyte of only 1 M $ZnSO_4$(aq). When 5.0% w/v SiO_2 was added into 1 M $ZnSO_4$(aq), see Figure (d), the number of cycles that the symmetrical Zn/Zn cell could sustain its cycling test was prolonged to more than 100 cycles. Soon afterwards, the 1 M $ZnSO_4$(aq) + 5.0% w/v SiO_2 system still short-circuited, even though the cycle number was double that of the system with 1 M $ZnSO_4$(aq). Regarding Fig. 3 (b) and (c), the voltage stability of the system that has 1 M $ZnSO_4$(aq) + either 0.5 or 1.0% w/v SiO_2 lasts much longer than 100 cycles, especially for the 1.0% w/v SiO_2 system in which there is no short-circuiting observed even the test completes 200 cycles.

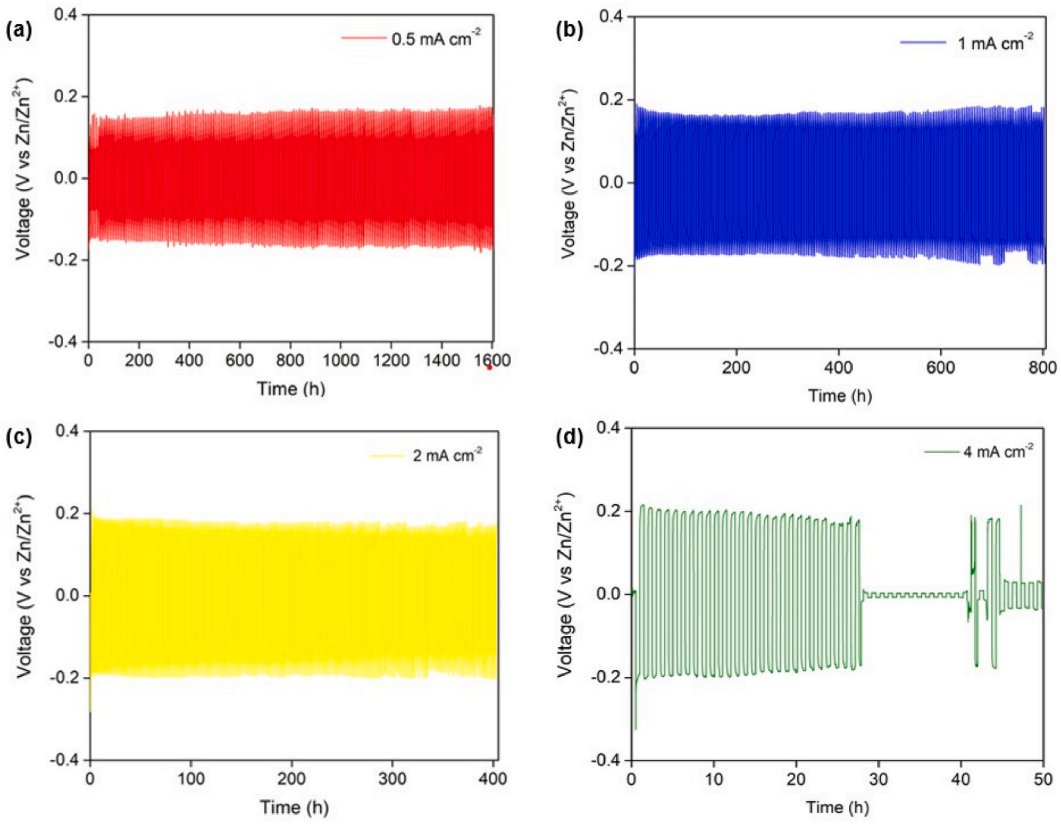

Fig. 2. Voltage profiles versus time of the Zn/Zn symmetric cells using 1 M $ZnSO_4$(aq) as the electrolyte when being cycling-tested at different current densities of (a) 0.5 mA cm^{-2}, (b) 1.0 mA cm^{-2}, (c) 2.0 mA cm^{-2}, and (d) 4.0 mA cm^{-2}.

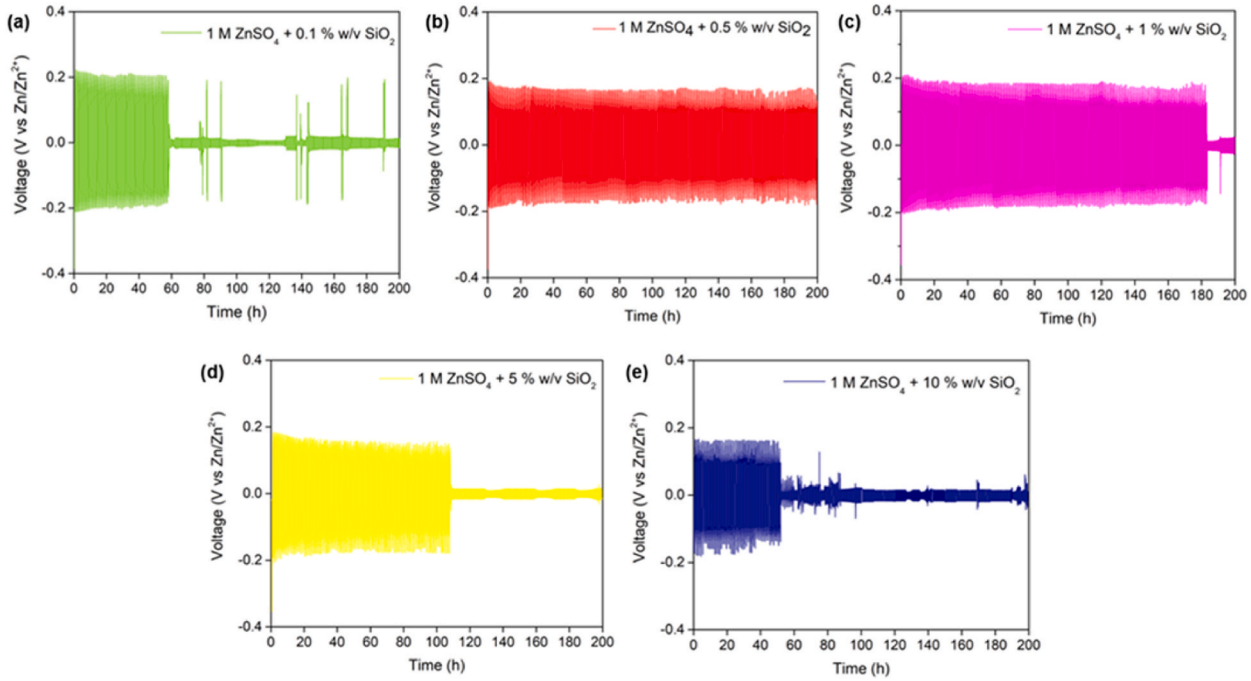

Fig. 3. Voltage profiles versus time of the Zn/Zn symmetric cells using 1 M $ZnSO_4$(aq) + x % w/v SiO_2 as the electrolyte: (a) x = 0.1, (b) x = 0.5, (c) x = 1.0, (d) x = 5.0, and (e) x = 10.0, when being cycling-tested at the different current density of 4.0 mA cm^{-2}.

Apparently, SiO_2 plays a role in uniformizing the Zn plating/stripping processes at the Zn/electrolyte interface. Yang et al. [25] reported that when using SiO_2-nanosphere-coated separator, oxygen atoms with negative polarity in SiO_2 lattice formed a network for Zn^{2+} transport channel by the electrostatic attraction between O and Zn. This network directed and enhanced migration of Zn^{2+}, resulting in homogeneous Zn plating and stripping. The chance of Zn-dendrite nucleation was therefore greatly reduced. For this reason, adding the specific content of SiO_2 of 0.5% w/v in the 1 M $ZnSO_4$(aq) electrolyte helps suppressing Zn dendritic formation and growth, as well as stabilizing the Zn/electrolyte interface. If the amount of SiO_2 in the electrolyte is too low (0.1% w/v), there may not be enough SiO_2 to functionalize as Zn^{2+}-transport-aiding network; 1 M $ZnSO_4$(aq) + 0.1% w/v SiO_2 is no difference from 1 M $ZnSO_4$(aq) in the sense of Zn plating/stripping. If the amount of amount of SiO_2 in the electrolyte is too high (10.0% w/v), the electrolyte may have less Zn^{2+}-conductive channel. Due to the fact that SiO_2 alone cannot conduct zinc-ions and SiO_2 is very hygroscopic, too many SiO_2 particles in the electrolyte can increase the electrolyte viscosity by adsorbing water molecules, and densely aggregate, lowering the electrolyte conductivity and subsequently inhibiting the movement of water molecules and (water-solvated) Zn ions. For this reason, it is highly possible for Zn dendrites to form and grow. What happens at the interface between the Zn electrode and the electrolyte system comprising 1 M $ZnSO_4$(aq) + x % w/v SiO_2 from morphological perspective will be discussed later.

On top of the electrochemical results or more precisely the voltage profile, operando optical microscopy was a chosen technique to visualize the Zn/electrolyte interface for further analysis during the cycling of Zn plating and stripping. The sequence of the cycling tests started with the plating and was followed by the stripping. The first set of analyzed systems was of the symmetrical Zn/Zn cells comprising 1 M $ZnSO_4$(aq) and undergoing the cycling tests at 0.5, 1.0, 2.0, or 4.0 mA cm^{-2} with the areal capacity of 2.0 mAh·cm^{-2}. The optical images at the interface of all the systems can be seen in Fig. 4. For the systems tested with the low current densities of 0.5 and 1.0 mA cm^{-2}, see Fig. 4 (a) and (b), during the plating/stripping of up to the 25th cycle, the Zn interface remains relatively smooth and close to the pristine state. From the 50th cycle onward, the interface becomes highly roughened and spiny, resulting from uneven Zn plating and stripping along the interface. Besides, corrosion and passivation of Zn electrode due to chemical reactions between Zn and water may be responsible for the localized plating and stripping. Considering Fig. 4 (c), when the current density of 2.0 mA cm^{-2} was used, the nucleation of Zn dendrites is observed in the 1st plating. After the 10th plating or stripping, the size of the Zn dendrites increases laterally and longitudinally, yet the dendrites exist around the interface as indicated by the yellow arrows in Fig. 4 (c). Interestingly, more dendrites continue to arise laterally but no longer grow longitudinally even after the 25th, 50th, and 100th cycles, respectively.

Apart from the dendrites, the Zn electrode appears rougher at the interface, but not as spiny as those of the previous cases with the low current densities (0.5 and 1.0 mA cm^{-2}). This may suggest that the Zn corrosion and passivation occurred at the lower extent because the cycling time for 2.0 mA cm^{-2} is only 400 h compared to 800 h for 1.0 mA cm^{-2} and 1600 h for 0.5 mA cm^{-2}. That no evidence of the Zn dendrites severely piercing into the separator is seen in the Zn/Zn cells cycled at lower than or equal to 2.0 mA cm^{-2} concurs with the steady voltage profiles that are formerly mentioned. Larger Zn dendrites are present at the interface of the system that was tested at 4.0 mA cm^{-2} from the 1st cycle. After the successive cycles (10th, 25th, and 50th cycles), the dendrites grow laterally and

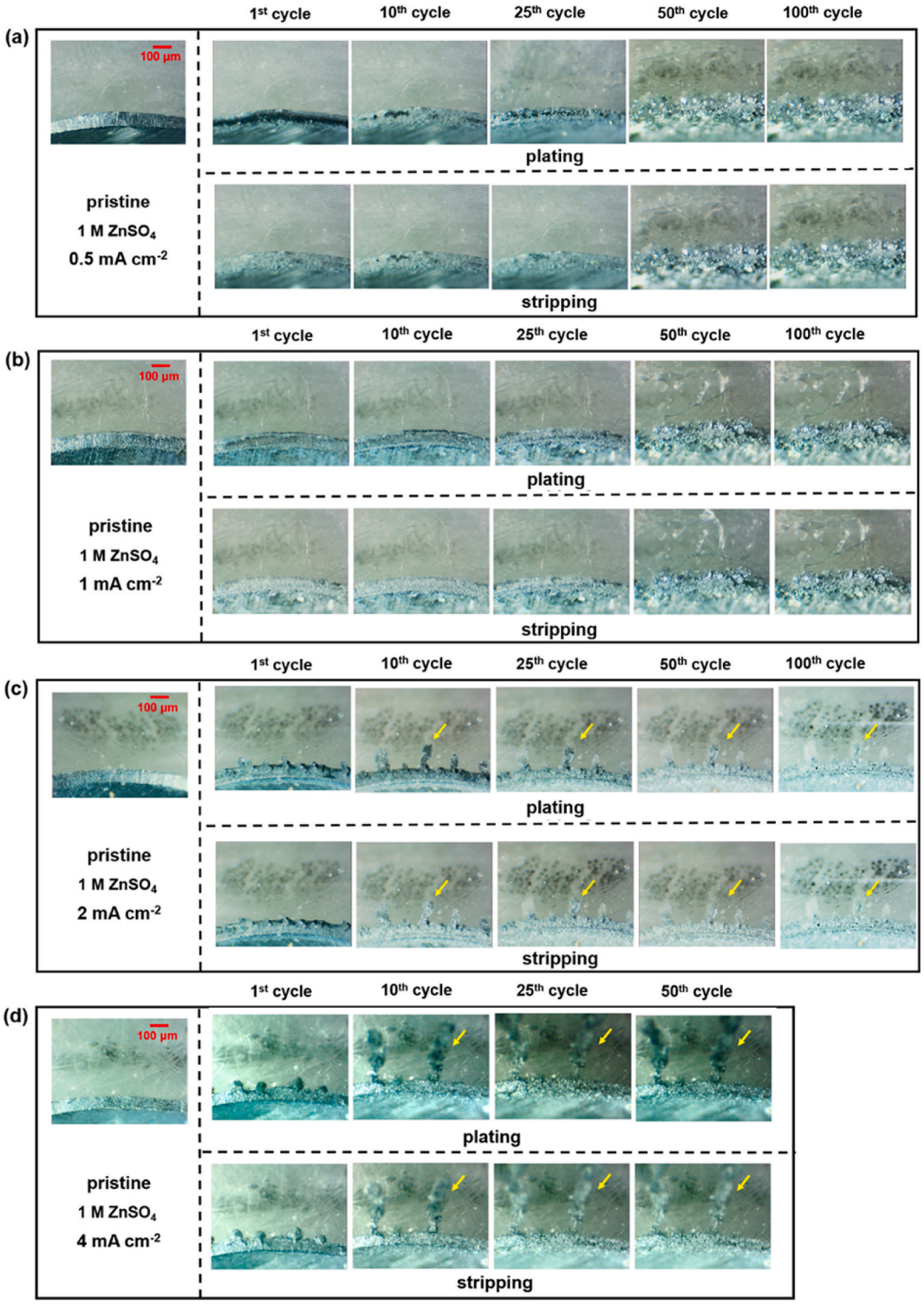

Fig. 4. Optical images at the interface between the Zn electrode and the electrolyte of 1 M $ZnSO_4$(aq) in the symmetric Zn/Zn cells taken by operando optical microscopy
during cycling at the different current densities (a) 0.5 mA cm^{-2}, (b) 1.0 mA cm^{-2},
(c) 2.0 mA cm^{-2}, and (d) 4.0 mA cm^{-2}.

especially longitudinally according to Fig. 4 (d), see the yellow arrows. It is obvious that the dendrites have the cactus-like structure, become larger, and penetrate farther into the separator when the cycle number increases. The dendrites not only go forward deeply, but they also highly likely connect to those initiated from the other Zn electrode ff the zero voltages or short-circuiting characteristics in Fig. 2 (d) are taken as the basis. VDO clips of the formation and growth of the Zn dendrites can be seen in the supplementary data section. The Zn electrode in the case of 4.0 mA cm^{-2} does not look as quite rough as that in the case of 2.0 mA cm^{-2} when considering the 50th cycle of plating and stripping possibly owing to less cycling time.

Though the operando optical microscopy provides "real-time" characterization, it can inspect the location just around the Zn/electrolyte interface. In order to cover the whole area of the separator with the Zn-dendrite formation and growth, the synchrotron X-ray imaging was performed with the stacks of Zn/separator/Zn from the symmetrical cells containing 1 M $ZnSO_4$(aq) and undergoing cycling tests at 0.5, 1.0, 2.0, or 4.0 mA cm^{-2} for 10, 50, and 100 cycles. For the low current densities (0.5 and 1.0 mA cm^{-2}), the X-ray imaging technique shows that there is no sign of Zn dendrites throughout the separator from the pristine state to 100 cycles of the electrochemical test as evidenced in Fig. 5 (a) to (h). This agrees with the operando optical images (Fig. 4 (a) & (b)) and the voltage profiles (Fig. 2 (a) & (b)). In case of 2.0 mA cm^{-2}, the X-ray imaging does not depict any Zn dendrites at the 10th cycle of the galvanostatic cycling, shown in Fig. 5 (i) & (j); however, the dendrites emerging near the Zn/separator (electrolyte) interface are detected in Fig. 5 (k) & (l), see the red arrows, when the cycling lasts for the 50 and 100 cycles. This is somewhat different from the optical interfacial images in which the dendrites are portrayed even at the 10th cycle and the following cycles. The reason why the X-ray imaging can exhibit the Zn dendrites only at the high number of cycles may relate to its lateral resolution; more Zn dendrites per the Zn electrode area or higher in the areal density of the dendrites are required to be detectable. With respect to Fig. 5 (n), the Zn dendrites are already observed around the Zn/separator interface at the 10th cycle of the 4.0-mA·cm^{-2}-test, when compared to the pristine state in Fig. 5 (m). More importantly, it is possible to witness the existence of the Zn dendrites all over the separator region as in Fig. 5 (o) when the test reaches the 50th cycle. This X-ray unfolding supports the previous deduction of short-circuiting as consequences of the Zn dendritic penetration through the separator and the direct connection between the two Zn electrodes via the Zn dendrites from both the electrochemical and operando optical characterizations, see Fig. 2 (d) and 4 (d).

Carrying on the microstructural analysis from the voltage profiles of the Zn/Zn cells with the electrolyte systems of 1 M $ZnSO_4$ + x % w/v SiO_2 that passed a series of cycling under 4.0 mA cm^{-2}, the operando optical images at the interface between the Zn electrode and the electrolyte (separator) are illustrated in Fig. 6. At the lowest content of SiO_2 (0.1% w/v) in the electrolyte, the long fern-like Zn dendritic bundles are displayed in Fig. 6 (a), specified by the yellow arrows, from the 10th to 100th cycles. As mentioned formerly, this SiO_2 content may be too little to effectively blocking the Zn dendritic formation and growth. The dendrites form and grow differently with no exact shapes even the cycling was performed for 100 cycles when more SiO_2 of 1.0 and 5.0% w/v were added into the

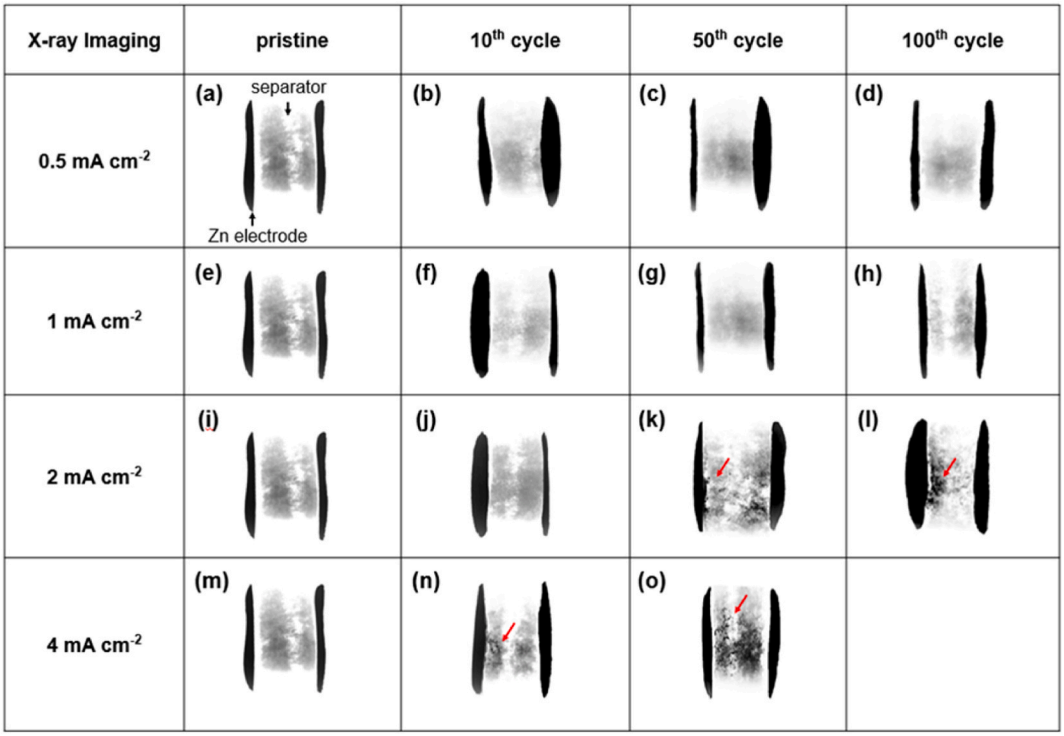

Fig. 5. X-ray imaging of the stacks of Zn/separator/Zn from the Zn/Zn symmetrical cells using the1 M $ZnSO_4$(aq) electrolyte and after undergoing cycling tests for 10, 50, and 100 cycles at different current densities: (a) to (d) 0.5 mA cm^{-2}, (e) to (h) 1.0 mA cm^{-2}, (i) to (l) 2.0 mA cm^{-2}, and (m) to (o) 4.0 mA cm^{-2}.

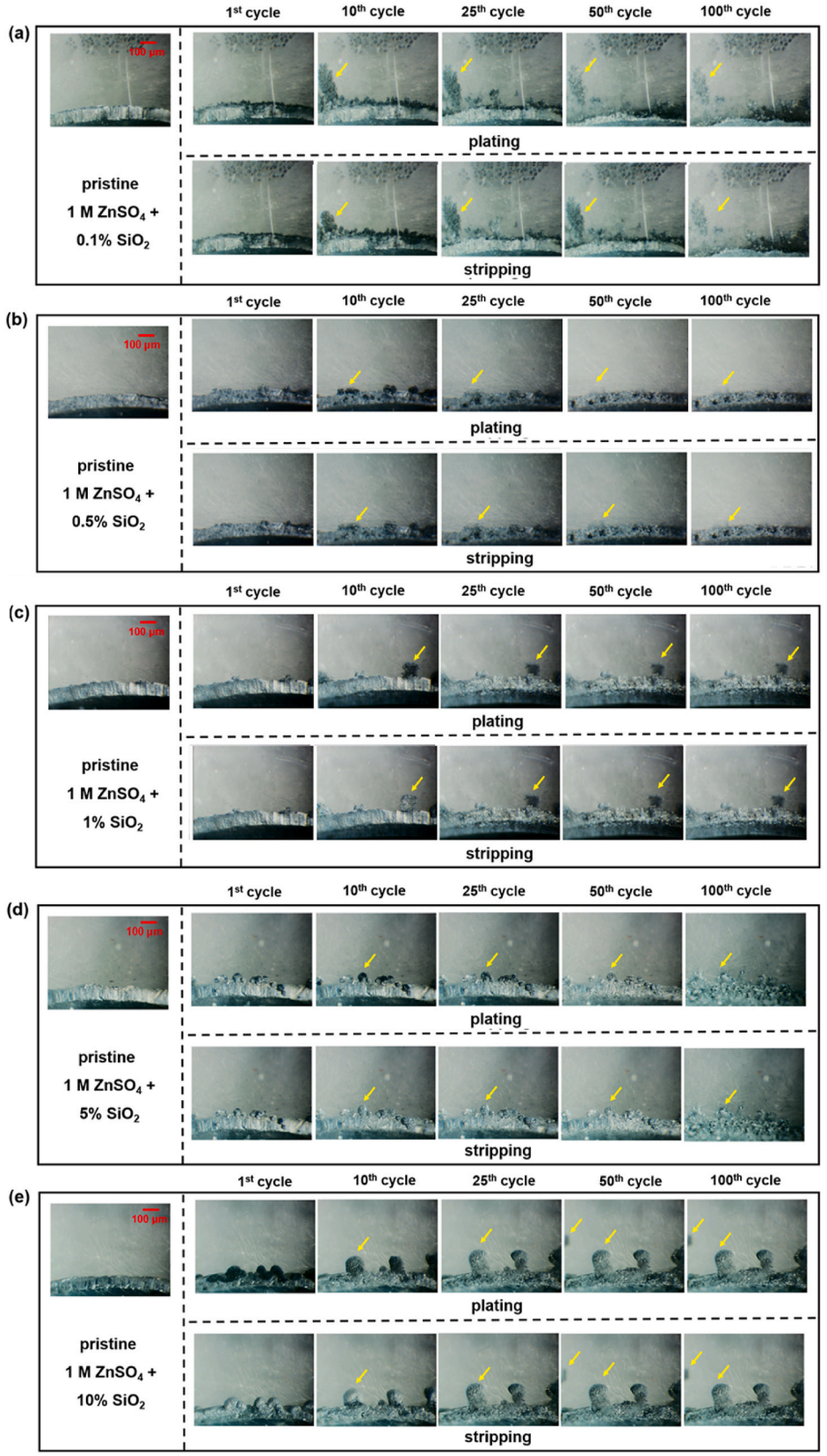

(caption on next page)

Fig. 6. Optical images at the interface between the Zn electrode and the electrolyte of 1 M $ZnSO_4$(aq) + x % w/v SiO_2 in the symmetric Zn/Zn cells: (a) x = 0.1, (b) x = 0.5, (c) x = 1.0, (d) x = 5.0, and (e) x = 10.0, taken by operando optical microscopy during cycling at the current density of 4.0 mA cm^{-2}.

electrolyte as can be distinguished in Fig. 6 (c) & (d). The dendrites are also accompanied with the Zn electrode roughening due to the reactions with water. In the particular case of 10% w/v SiO_2, the dendrites look more like rounded columns and several of them are clearly formed along the interface from the 10th cycle onwards as in Fig. 6 (e).

All these SiO_2-added electrolyte systems link to the formation and growth of the Zn dendrites, and eventually short-circuiting of the Zn/Zn cells as stated by the voltage polarizations in Fig. 3 (a) and 3 (c)–(e). At the specific 0.5% w/v SiO_2 in 1 M $ZnSO_4$, Zn dendrites do rise up at the Zn/electrolyte interface but limitedly form near to the Zn electrode, turning the pristine interface to be hilly after the 100th cycle of the Zn plating and stripping, see Fig. 6 (b). In other words, the Zn plating and stripping processes at such a high current density of 4.0 mA cm^{-2} are reversible. Moreover, the interface does not represent high degree of roughness potentially associating with an additional function of SiO_2 of the Zn electrode protection from corrosion and passivation relating to reactions with water. These findings confirm the positive effects of this SiO_2 quantity, which coincides with the electrochemical cycling data in Fig. 3 (b).

The surface of the Zn electrodes from the Zn/Zn cells that used the electrolyte systems of 1 M $ZnSO_4$(aq) or 1 M $ZnSO_4$(aq) + 0.5% w/v SiO_2 were cycled at 4.0 mA cm^{-2} after different cycles (10, 25, and 50 cycles) of the Zn plating and stripping was analyzed by Raman spectroscopy as shown in Fig. 7 (ab) and (b). The analysis mainly aims to verify the causes of the Zn dendritic formation and growth, and short circuiting. It is presumed that the corrosion and passivation of metallic Zn as a result of interaction with water may correlate to such phenomena. Besides, SiO_2 may has a distinctive role in alleviating the negative consequences of the Zn-water interaction in addition to the role of homogenizing the movement of Zn ions and the electrochemical reactions of Zn ions.

Regarding Fig. 7 (a), one of the obtained main functional groups on the Zn surface from the 1 M $ZnSO_4$(aq) electrolyte is ZnO existing from the Zn–O peaks corresponding to the wave number between 400 and 450 cm^{-1} and the one at around 1140 cm^{-1}. Another main functional group found is $\mathbf{SO_4^{2-}}$ (using Zn$\mathbf{SO_4}$ as a reference) at the approximate wave number of 972 cm^{-1}. From this SO_4^{2-} group, it can be inferred to the so called $Zn_4(OH)_6SO_4$ that was proposed to exist on the Zn surface after being in contact with an aqueous $ZnSO_4$ electrolyte [18]. Note that there is no standard compound of $Zn_4(OH)_6SO_4$ available as a reference for the Raman measurement. The –OH group from either $Zn(OH)_2$ or $Zn_4(OH)_6SO_4$ at the wave number between 3300 and 3400 cm^{-1}. The Raman spectra intensities of those ZnO, –OH, and SO_4^{2-} peaks are amplified versus the number of plating and stripping cycles, signifying more $Zn_4(OH)_6SO_4$, ZnO, and $Zn(OH)_2$ accumulate on the Zn surface. As all the zinc compounds are of electronically insulating nature, they cause the Zn electrode surface to be less electronically conductive and subsequently less accessible area for the electrochemical reactions of Zn plating and stripping. This accordingly boosts the localized current density at the diminished reaction area and prompts the growth of the Zn dendrites towards short circuiting. The ZnO, –OH, and SO_4^{2-} peaks of the Zn electrode surface from the 1 M $ZnSO_4$(aq) electrolyte with the addition of 0.5% w/v SiO_2 are likewise located at almost the same wave numbers, see Fig. 7 (b).

As a fascinating effect of the SiO_2 additive into 1 M $ZnSO_4$(aq), the Raman peaks' intensities for ZnO, –OH, and SO_4^{2-} at the 10th, 25th, and even 50th cycle of the plating and stripping are significantly lower in comparison to the case of the 1 M $ZnSO_4$(aq) electrolyte. Notably, Si–O peaks from SiO_2 are rarely visible on the Zn surface in the Raman spectra, describing that SiO_2 did not cover on the surface and hindered the relevant electrochemical reactions. It can be instead expressed that SiO_2 particles (at the 0.5 w/v % content) preferably disperse in the aqueous 1 M $ZnSO_4$, attenuate the passivation of $Zn_4(OH)_6SO_4$, ZnO, and $Zn(OH)_2$ [18] as well as prevent the Zn electrode corrosion as coincided with the close-to-pristine Zn/electrolyte interface after being long-time cycled in Fig. 6 (b). The role of SiO_2 on suppressing the formation of the insulating compounds of ZnO or $Zn(OH)_2$ or $Zn_4(OH)_6SO_4$ is not yet completely understood. SiO_2 may deactivate the active H_2O molecules to react with the Zn electrode similarly to other additives like dimethyl sulfoxide, ammonium chloride, or ethylamine hydrochloride as reported by Refs. [27–35].

The presence of the passivation compounds of ZnO and particularly $Zn_4(OH)_6SO_4$ on the Zn electrode after being cycled at 4.0 mA cm^{-2} for 50 cycles in the electrolyte case of 1 M $ZnSO_4$(aq)were well confirmed (on top of the Raman detection) by the XRD patterns in Fig. 7 (c). The peak intensities related to $Zn_4(OH)_6SO_4{\cdot}xH_2O$ are the most pronounced, followed by those of ZnO, along with $Zn(OH)_2$. Both the accompanied ZnO and $Zn(OH)_2$ are seen with quite low intensities. According to these XRD recognitions, significantly thick layer of combined $Zn_4(OH)_6SO_4$, ZnO, and $Zn(OH)_2$ formed on the surface of the Zn electrode. Interestingly, the Zn electrode after being cycled at 4.0 mA cm^{-2} for 50 cycles in 1 M $ZnSO_4$(aq) + 0.5% w/v SiO_2 shows almost the same XRD patterns as the pristine Zn electrode. This observation plus the previous Raman spectra suggests limited formation of $Zn_4(OH)_6SO_4$, ZnO, and $Zn(OH)_2$; in other words, thin layer of such passivation species covered the Zn surface as SiO2 can improve the surface quality of the Zn electrode by soothing the undesirable interactions between the Zn electrode and the aqueous electrolyte. Note that the XRD results of the Zn electrode after being cycled at 4.0 mA cm^{-2} for less than 50 cycles were not included as the peak intensities of any surface species were extremely low and not observable.

The SEM micrographs in Fig. 8 illustrate the surface morphology of the Zn electrode at different conditions. For the pristine Zn electrode in Fig. 8 (a)–(b), the surface is relatively smooth without any coverage; some micro-sized splits and lines can be seen possibly as a result of the manufacturing process. After being cycled at 4.0 mA cm^{-2} for 50 cycles as in the Zn/Zn cells with the 1 M $ZnSO_4$(aq) electrolyte, the Zn surface in Fig. 8 (c)–(d) became clearly roughened and was covered with flaky substances, which were highly likely the surface passivation species of $Zn_4(OH)_6SO_4$, ZnO, and $Zn(OH)_2$ as indicated by the Raman and XRD detection, or possibly the Zn dendritic structure according to the formation of Zn dendrites as pointed out by the short-circuiting voltage profile and the X-ray imaging. In case of the 1 M $ZnSO_4$(aq) + 0.5% w/v SiO_2 electrolyte, the Zn electrode surface that was cycled 4.0 mA cm^{-2} for 50 cycles appear much more comparably to that of the pristine electrode, though the surface looks slightly corroded as well as scarcely and

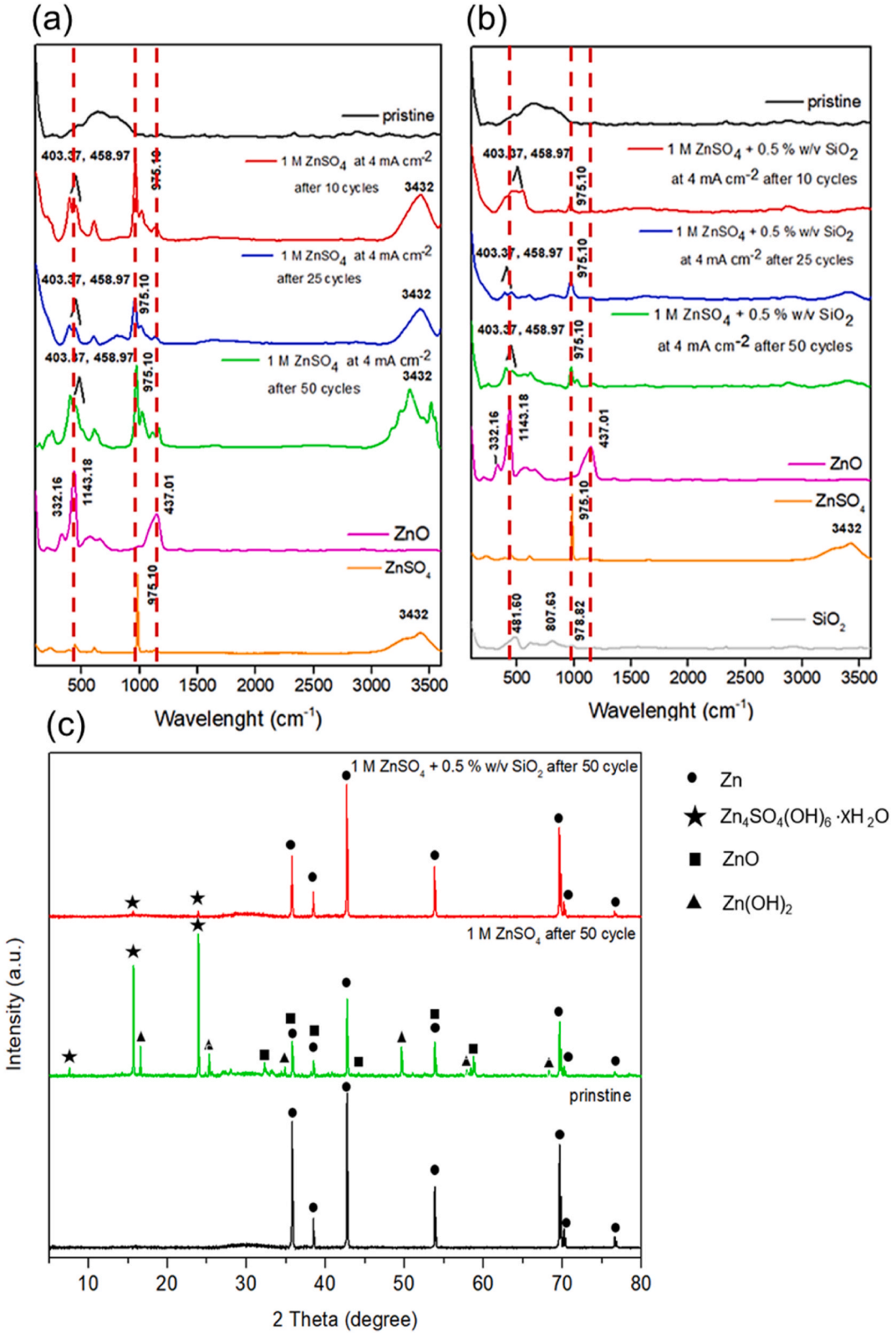

(caption on next page)

Fig. 7. Raman spectra of the Zn electrode from the symmetrical Zn/Zn cells using the electrolyte of (a) 1 M $ZnSO_4$(aq) or (b) 1 M $ZnSO_4$(aq) + 0.5% w/v SiO_2 and undergoing the cycling test at 4.0 mA cm^{-2} for 10, 25, and 50 cycles, and (c) XRD patterns of the pristine Zn electrode and the Zn electrode from the symmetrical Zn/Zn cells with the electrolyte of 1 M $ZnSO_4$(aq) and 1 M $ZnSO_4$(aq) + 0.5% w/v SiO_2 undergoing the cycling test at 4.0 mA cm^{-2} for 50 cycles.

scatteringly concealed with some substances, very likely to be the mentioned passivation species. Again, this is in line with the Raman and XRD results that limited passivation species should be present in the case of SiO_2-containing electrolyte.

When the data from Figs. 7 and 8 are considered simultaneously, all the Raman, XRD, and SEM techniques coherently support that the surface passivation species were significantly formed on the cycled Zn electrode in the 1 M $ZnSO_4$(aq) electrolyte and these species were formed on the cycled Zn electrode in the 1 M $ZnSO_4$(aq) + 0.5% w/v SiO_2 electrolyte at the limited extent thanks to the fact that SiO_2 did restrict such a formation, see Fig. 8 (e)–(f). That SiO_2 can restrict the formation of the passivation (insulating) species on the Zn surface is responsible for better cyclability of the Zn/Zn cells at the high current density with the 1 M $ZnSO_4$(aq) + 0.5% w/v SiO_2

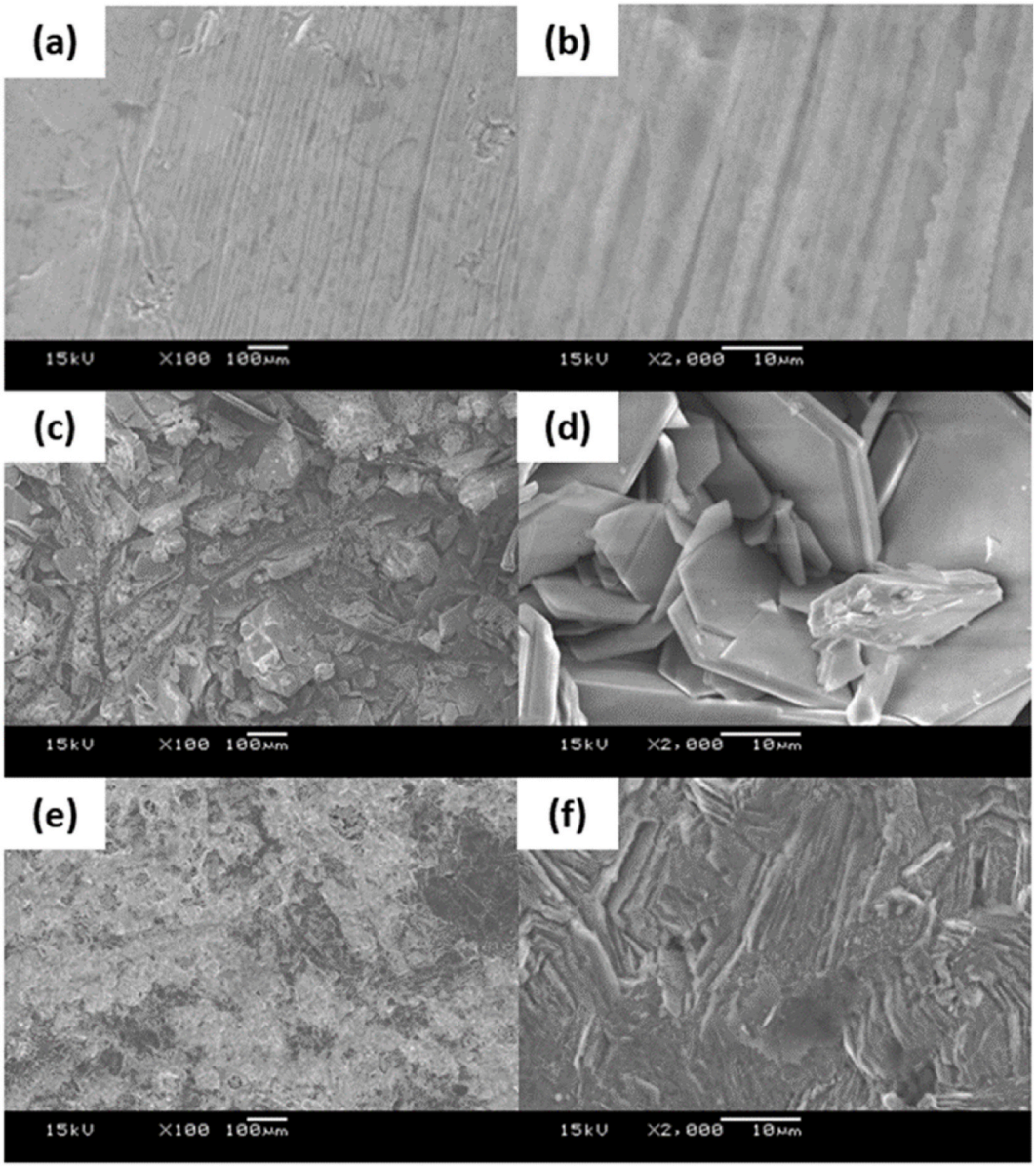

Fig. 8. SEM images of the pristine Zn electrode surface (a)–(b), and the Zn electrode surface from the symmetrical Zn/Zn cells using the electrolyte of
(c) – (d) 1 M $ZnSO_4$(aq), or (e)–(f) 1 M $ZnSO_4$(aq) + 0.5% w/v SiO_2,
and undergoing the cycling test at the current density of 4.0 mA cm^{-2} for 50 cycles.

electrolyte as the surface of the Zn electrode is nearly at the pristine state, making the whole surface area more active and accessible for the Zn plating and stripping unlike the Zn surface in the 1 M $ZnSO_4$(aq) electrolyte that was strongly hindered by the passivation species. Above all, these outcomes have encouraged the utilization of SiO_2 as an effective and low-cost additive to enhance the surface quality of the Zn electrode as well as to suppress the Zn dendrites when being applied in the aqueous Zn-ion batteries. Moreover, in the future works, construction of full Zn-ion battery cells that consist of proper positive electrodes like MnO_2, V_2O_5, or CuHCF (HCF = hexacyanoferrate) can be expected of long-term stable Zn electrode and long-lasting high-performance batteries.

4. Conclusions

It is found out that the higher current density the symmetrical Zn/Zn cells with 1 M $ZnSO_4$(aq) are electrochemically tested of the cyclic Zn plating and stripping, the higher chance the Zn dendrites can grow. At the worst case of 4.0 mA cm^{-2}, the dendrites do intrude the separator and create direct electrical contact between the two Zn electrodes, leading to short-circuiting. This behavior is ascertained by the electrochemical voltage profile, the operando optical imaging, as well as the synchrotron X-ray imaging. Adding the definite quantity of 0.5 %w/v SiO_2 into 1 M $ZnSO_4$(aq) favorably restrict not only the intrusion of the Zn dendrites farther into the separator, but also the corrosion and passivation of the Zn electrode surface. The stable cycling voltage profile and the operando optical interfacial images advocate the former claim. The latter claim results from both the operando optical imaging and ex-situ Raman, XRD, and SEM analyses at the Zn/electrolyte interface and the Zn electrode surface, respectively. The interface at the cycled and pristine states looks quite alike, and surface passivation species of $Zn_4(OH)_6SO_4$, ZnO, and $Zn(OH)_2$ are detected at little amount on the cycled Zn electrode. Owing to the electronically insulating nature of the passivation species, when they cover the Zn electrode surface, the active surface area for the Zn plating and stripping would be lower. This limited active area on the Zn electrode can lead to the strong concentration of the localized current density as well as the confined space of the Zn plating, which is a critical condition to stimulate the Zn dendritic formation and growth. Thereby, it can be deducted that this surface passivation is another possible root of such undesirable issue of the Zn dendrites, more precisely the short-circuiting behavior. All in all, the SiO_2 additive has 2 main functions: i) promotion of Zn^{2+} mobility for the electrochemical reactions at the Zn/electrolyte interface and ii) suppression of the formation of insulating layer on the Zn electrode surface. This information has not been previously introduced in the other works related to the short-circuiting failure of Zn-ion batteries.

Author contribution statement

Pornnapa Phummaree: Conceived and designed the experiments; Performed the experiments; Wrote the paper.
Manaswee Suttipong: Conceived and designed the experiments; Analyzed and interpreted the data.
Theeraboon Jaroonsteanpong: Performed the experiments.
Catleya Rojviriya: Performed the experiments; Analyzed and interpreted the data.
Rojana Pornprasertsuk, Soorathep Kheawhom: Analyzed and interpreted the data.
Jitti Kasemchainan: Conceived and designed the experiments; Analyzed and interpreted the data; Wrote the paper.

Data availability statement

The data that has been used is confidential.

Declaration of competing interest

The authors declare that they have no known competing financial interests or personal relationships that could have appeared to influence the work reported in this paper.

Acknowledgements

This work was financially supported by Office of the Permanent Secretary, Ministry of Higher Education, Science, Research, and Innovation with Grant No. RGNS 63-012 for research consumables and analytical fees. This work was also supported by Ratchadapisek Somphot Fund, Chulalongkorn University for research equipment. Lastly, the Program Management Unit for Human Resources & Institutional Development, Research and Innovation (B16F640166) is acknowledged for the research assistantship and the travel and subsistence expenses related to the research exchange and conference.

References

[1] N. Zhang, X. Chen, M. Yu, Z. Niu, F. Cheng, J. Chen, Materials chemistry for rechargeable zinc-ion batteries, Chem. Soc. Rev. 49 (2020) 4203, https://doi.org/10.1039/c9cs00349e.
[2] W. Yutong, N. Liu, Visualizing battery reactions and processes by using in situ and in operando microscopies, Chem 4.3 (2018) 38–465, https://doi.org/10.1016/j.chempr.2017012.022.
[3] H. Dong, J. Li, S. Zhao, F. Zhao, J. Dan, L. Breet, G. He, S. Xiong, I.P. Parkin, An anti-aging polymer electrolyte for flexible rechargeable zinc-ion batteries, J. Mater. Chem. 8 (43) (2022) 2637–22644, https://doi.org/10.1039/D0TA07086F.

[4] Z. Zhang, S. Said, K. Smith, Y.S. Zhang, G. He, R. Jervis, P.R. Shearing, T.S. Miller, D.J.L. Brett, Dendrite suppression by anode polishing in zinc-ion batteries, J. Mater. Chem. 9 (27) (2021) 15355–15362, https://doi.org/10.1039/D1TA02682H.

[5] J. Yi, P. Liang, X. Liu, K. Wu, Y. Liu, Y. Wang, Y. Xia, J. Zhang, Challenges, migration strategies and perspectives in development of zinc-electrode materials and fabrication for rechargeable zinc-air batteries, Energy Environ. Sci. 11 (2018) 3075, https://doi.org/10.1039/C8EE01991F.

[6] Y. Zuo, K. Wanh, P. Pei, M. wei, X. Liu, Y. Wiao, P. Zhang, Zinc dendrite growth and inhibition strategies, Mater. Today Energy 20 (2021), 100692, https://doi.org/10.1016/j.mtener.2021.100692.

[7] H. Qiu, X. Du, J. Zhao, Y. Wang, J. Ju, Z. Chen, Z. Hu, D. Yan, X. Zhou, G. Cui, Zinc anode-compatible in-situ solid electrolyte interphase via cation solvation modulation, Nat. Commun. 10 (1) (2019) 5374, https://doi.org/10.1038/s41467-019-13436-3.

[8] Y. Yang, X. Liu, Z. Dai, F. Uuan, Y. Bando, D. Golberg, X. Wang, In situ electrochemistry of rechargeable battery materials: status report and perspectives, Adv. Mater. 29 (31) (2017), 1606922, https://doi.org/10.1002/adma.201606922.

[9] Z. Zhao, J. Zhao, Z. Hu, J. Ji, Y. Zhang, C. Wang, G. Cui, Long-life and deeply rechargeable aqueous Zn anodes enabled by a multifunctional brightener-inspired interphase, Energy Environ. Sci. 2 (6) (2019) 1938–1949, https://doi.org/10.1039/C9EE00596J.

[10] S.J. Banik, R. Akolkar, Suppressing dendritic growth during alkaline zinc electrodeposition using polyethyleneimine additive, Electrochim. Acta 179 (2015) 475–481, https://doi.org/10.1016/j.electacta.2014.12.100.

[11] V. Yufit, F. Tariq, D.S. Eastwood, M. Biton, B. Wu, P.D. Lee, N.P. Brandon, Operando visualization and multi-scale tomography studied of dendrite formation and dissolution in zinc batteries, Joule 3 (2) (2019) 485–502, https://doi.org/10.1016/j.joule.2018.11.002.

[12] Z. Cai, J. Wang, Z. Lu, R. Zhan, Y. Ou, L. Wang, M. Dahbi, J. Alami, J. Lu, K. Amine, Y. Sun, Ultrafast metal electrodeposition revealed by in situ optical imaging ang theoretical modeling toward fast-charging Zn battery chemistry, Angew. Chem. 134 (14) (2022), e220116560, https://doi.org/10.1002/ange.202116560.

[13] X.S. Lin, Z.R. Wang, L.H. Ge, J.W. Xu, M.M. Ren, W.L. Lu, J.S. Yao, C.B. Zhang, Electrolyte modefication for long-life Zn ion batteries: achieved by methanol additive, Chemelectrochem 9 (4) (2022), e2021724, https://doi.org/10.1002/celc.202101724.

[14] J. Hao, X. Li, S. Zhang, F. Yang, X. Zeng, S. Zhang, G. Bo, C. Wang, Z. Guo, Designing dendrite-free zinc anodes for advanced aqueous zinc batteries, Adv. Funct. Mater. 30 (30) (2022), 2001263, https://doi.org/10.1002/adfm.202001263.

[15] S. Liu, J. Mao, W.K. Pang, J. Voongsviivut, X. Zeng, L. Thomsen, Y. Wang, J. Liu, D. Li, Z. Guo, Tuning the electrolyte solvation structure to suppress cathode dissolution, water reactivity, and Zn dendrite growth in zinc-ion batteries, Adv. Funct. Mater. 31 (38) (2021), 2104281, https://doi.org/10.1002/adfm.202104281.

[16] H. Yang, Y. Qiao, Z. Chang, H. Deng, P. He, H. Zhou, A Metal-Organic Framework as a multifunctional ionic sieve membrane for long-life aqueous zinc-iodide batteries, Adv. Mater. 32 (38) (2020), e2004240, https://doi.org/10.1002/adma.202004240.

[17] H. Qiu, X. Du, J. Zhao, Y. Wang, J. Ju, Z. Hu, D. Yan, X. Zhou, G. Cui, Zinc anode-compatible in-situ solid electrolyte interphase via cation solvation modulation, Nat. Commun. 10 (1) (2019) 5374, https://doi.org/10.1038/s41467-019-13436-3.

[18] J. Yang, J. Cao, Y. Peng, W. Yang, S. Barg, Z. Liu, I.A. Kinloch, M.A. Bissett, R.A.W. Dryfe, Unravelling the mechanism of rechargeable aqueous Zn–MnO2 batteries: implementation of charging process by electrodeposition of MnO2, ChemSusChem 13 (2020) 4103–4110, https://doi.org/10.1002/cssc.202001216.

[19] Y. Jin, K.S. Han, Y. Shao, M.L. Sushko, J. Xiao, H. Pan, J. Liu, Stabilizing zinc anode reactions by polyethylene oxide polymer in mild aqueous electrolytes, Adv. Funct. Mater. 30 (2022), 2003932, https://doi.org/10.1002/adfm.202003932.

[20] W. Yan, Z. Zhaohua, D. Shen, L. Chen, T. Song, T. Kang, Z. Tong, Y. Tang, H. Wui, C.S. Lee, Electrolyte engineering enables stable Zn-ion deposition for long-cycling life aqueous Zn-ion batteries, Energy Storage Mater. 45 (2022) 1084–1091, https://doi.org/10.1016/j.ensm.2021.11.003.

[21] C. Liu, Y. Tian, Y. An, Q. Yang, S. Xiong, J. Feng, Y. Qian, Robust and flexible polymer/MXene-derived two dimensional TiO_2 hybrid gel electrolyte for dendrite-free solid-state zinc-ion batteries, Chem. Eng. J. 403 (2022), 132748, https://doi.org/10.1016/j.cej.2021.132748.

[22] M. Johnsi, S. Austin Suthanthiraraj, Compositional effect of ZrO_2 nanofillers on a PVDF-co-HFP based polymer electrolyte system for solid state zinc batteries, Chin. J. Polym. Sci. 34 (2016) 332–343, 10.1007/s10118-016-1750-3.

[23] R. Polu, A. Ranveer Kumar, Effect of Al_2O_3 ceramic filler on PEG-based composite polymer electrolytes for magnesium batteries, Adv. Mater. Lett. 4 (7) (2013) 543–547, https://doi.org/10.5185/amlett.2012.9417.

[24] A. Christina Nancy, S. Austin Suthanthiraraj, Effect of Al_2O_3 nanofiller on the electrical, thermal and structural properties of PEO: PPG based nanocomposite polymer electrolyte, Ionics 23 (2017) 1469, https://doi.org/10.1007/s11581-017-1976-2, 1449.

[25] P. Tian, X. Zhong, C. Gu, Z. Wang, F. Shi, SiO_2-alginate-based gel polymer electrolytes for zinc-ion batteries, Batteries 8 (10) (2022) 175, https://doi.org/10.3390/batteries8100175.

[26] Y. Yang, T. Chen, M. Zhu, G. Gao, Y. Wang, Q. Nie, Y. Jiang, T. Xiong, W.S. Lee, J. Xue, Regulating dendrite-free Zn deposition by a self-assembled OH-terminated SiO_2 nanosphere layer toward a Zn metal anode, ACS Appl. Mater. Interfaces 14 (33) (2022) 37759–37770, https://doi.org/10.1021/acsami.2c09144.

[27] Q. Zhang, Y. Ma, Y. Lu, X. Zhou, L. Lin, L. Li, Z. Yan, Q. Zhao, K. Zhang, J. Chen, Designing anion-type water-free Zn2+ solvation structure for robust Zn metal anode, Angew. Chem. Int. Ed. 60 (2021) 23357–23364, https://doi.org/10.1002/anie.202109682.

[28] F. Wang, O. Borodin, T. Gao, X. Fan, W. Sun, F. Han, A. Faraone, J.A. Dura, K. Xu, C. Wang, Highly reversible zinc metal anode for aqueous batteries, Nat. Mater. 17 (2018) 543–549, https://doi.org/10.1038/s41563-018-0063-z.

[29] J.F. Parker, C.N. Chervin, I.R. Pala, M. Machler, M.F. Burz, J.W. Long, D.R. Rolison, Rechargeable nickel–3D zinc batteries: an energy-dense, safer alternative to lithium-ion, Science 356 (2017) 415–418, https://doi.org/10.1126/science.aak9991.

[30] Y. Wang, Z. Wang, F. Yang, S. Liu, S. Zhang, J. Mao, Z. Guo, Electrolyte engineering enables high performance zinc-ion batteries, Small 18 (2022) 1–20, https://doi.org/10.1002/smll.202107033.

[31] L. Qian, H. Zhu, T. Qin, R. Yao, J. Zhao, F. Kang, C. Yang, Ultralow-salt-concentration electrolyte for high-voltage aqueous Zn metal batteries, Adv. Funct. Mater. 2301118 (2023) 1–9, https://doi.org/10.1002/adfm.202301118.

[32] L. Cao, D. Li, E. Hu, J. Xu, T. Deng, L. Ma, Y. Wang, X.-Q. Yang, C. Wang. Solvation structure design for aqueous Zn metal batteries. J. Am. Chem. Soc. 142 (220) 21404 https://doi.org/10.1021/jacs.0c09794.

[33] W. Kao-ian, M.T. Nguyen, T. Yonezawa, R. Pornprasertsuk, J. Qin, S. Siwamogsatham, S. Kheawhom, Highly stable rechargeable zinc-ion battery using dimethyl sulfoxide electrolyte, Mater. Today Energy 21 (2021), 100738, https://doi.org/10.1016/j.mtener.2021.100738.

[34] N. Chang, T. Li, R. Li, S. Wang, Y. Yin, H. Zhang, X. Li, An aqueous hybrid electrolyte for low-temperature zinc-based energy storage devices, Energy Environ. Sci. 13 (2020) 3527, https://doi.org/10.1039/D0EE01538E.

[35] R. Qin, Y. Wang, M. Zhang, Y. Wang, S. Ding, A. Song, H. Yi, L. Yang, Y. Song, Y. Cui, J. Liu, Z. Wang, S. Li, Q. Zhao, F. Pan, Tuning Zn2+ coordination environment to suppress dendrite formation for high-performance Zn-ion batteries, Nano Energy 80 (2021), 105478, https://doi.org/10.1016/j.nanoen.2020.105478.

[36] M. Ebner, F. Geldmacher, F. Marone, M. Stampanoni, V. Wood, X-ray tomography of porous, transition metal oxide-based lithium-ion battery electrodes, Adv. Energy Mater. 3 (7) (2013) 845–850, https://doi.org/10.1002/aenm.201200932.